Photocatalytic decolorization of bromothymol blue using biogenic selenium nanoparticles synthesized by terrestrial actinomycete *Streptomyces griseobrunneus* strain FSHH12

Atefeh Ameri[a], Mojtaba Shakibaie[b,*], Alieh Ameri[c], Mohammad Ali Faramarzi[d], Bagher Amir-Heidari[b], Hamid Forootanfar[e,*]

[a]Pharmaceutics Research Center, Institute of Neuropharmacology, Kerman University of Medical Sciences, Kerman, Iran, Tel. +98 34 31325238; Fax: +98 34 31325003; email: ameri1363@gmail.com
[b]Faculty of Pharmacy, Department of Pharmaceutical Biotechnology, Kerman University of Medical Sciences, Kerman, Iran, Tel. +98 34 31325253; Fax: +98 34 31325003; emails: mojtabashakibaie@yahoo.com, shakiba@kmu.ac.ir (M. Shakibaie), Tel. +98 34 31325001; Fax: +98 34 31325003; email: baheidari@yahoo.com (B. Amir-Heidari)
[c]Faculty of Pharmacy, Department of Medicinal Chemistry, Kerman University of Medical Sciences, Kerman, Iran, Tel. +98 34 31325238; Fax: +98 34 31325003; email: ameri60@gmail.com
[d]Faculty of Pharmacy and Biotechnology Research Center, Department of Pharmaceutical Biotechnology, Tehran University of Medical Sciences, Tehran, Iran, Tel./Fax: +98 21 66954712; email: faramarz@tums.ac.ir
[e]Herbal and Traditional Medicines Research Center, Kerman University of Medical Sciences, Kerman, Iran, Tel. +98 34 31325253; Fax: +98 34 31325003; email: h_forootanfar@kmu.ac.ir

Received 21 August 2015; Accepted 17 November 2015

ABSTRACT

The aim of the present study was to isolate and identify a terrestrial actinomycete bacterial strain capable to produce selenium nanoparticles (Se NPs) followed by purification of the biogenic Se NPs and evaluation of their photocatalytic degradation compared to selenium dioxide. Among 30 actinomycete bacterial strains obtained from environmental soil samples, one isolate (identified as *Streptomyces griseobrunneus* strain FSHH12 based on the 16S rDNA gene sequence analysis) was selected and used for production of Se NPs. The biologically synthesized Se NPs was consequently purified by an organic–aqueous partitioning system and characterized using scanning electron microscopy, transmission electron microscopy, energy dispersive X-ray, UV–visible spectroscopy, Fourier transform infrared spectroscopy, and X-ray diffraction spectroscopy. The obtained results of photocatalytic degradation of bromothymol blue using the purified Se NPs (64 µg/mL) revealed 62.3% of dye removal under UV illumination (15 W) after 60 min incubation of dye solution.

Keywords: Photocatalytic degradation; *Streptomyces griseobrunneus*; Selenium nanoparticles; Biosynthesis

*Corresponding authors.

1. Introduction

Large amounts of synthetic dyes including the azo, anthroquinone, and triphenylmethane dyes (TPMs) (based on the chemical structure of the chromophoric group) which are highly resistant to environmental breakdown have been increasingly produced and applied in the textile, paper, leather, pharmaceutical, cosmetic, and food industries [1–3]. TPMs identified as aromatic xenobiotic compounds to be highly toxic, mutagenic, and carcinogenic to the humans and animals [4]. Such environmentally hazardous properties together with their stability to sunlight has limited the application of TPMs as dyeing agent and prohibited their usage especially in aquaculture and food industries [4,5]. So, the wastewater containing dyes require proper treatment before being discharged into the environment [6].

Different processes including physical separation methods (flocculation, adsorption, coagulation, and membrane filtration, etc.), chemical approaches (like electrochemical treatment or ozonation), and biological techniques (either using microorganisms or enzymes) have been developed for decolorization and degradation of colorants [7,8]. Advanced oxidation processes (AOPs), such as Fenton's oxidation, ozonation, photocatalytic oxidation, and sonolysis have been widely used to treat wastewaters containing dyes [9–11]. AOPs associated with UV light and semiconductors such as titanium, zinc, cadmium, etc. have been applied to convert dye molecules on the basis of the creation of hydroxyl radicals ($\cdot$OH) in aqueous medium [9,12,13]. In fact, photocatalytic process along with UV radiation formed a redox environment in aqueous solution and usually decomposed the desired pollutant into water and carbon dioxide [14,15]. There are many reports on the application of photocatalytic approach in the presence of metal oxides and sulfides such as TiO_2, ZnO, WO_3, Fe_2O_3, ZnS, and CdS at nanoscale as nanocatalysts for the removal of xenobiotics [11,16]. Semiconductor chalcogens such as selenium (Se) have been also used for elimination of different dye groups due to their excellent physical characteristics like thermo-conductivity, anisotropy, and high photoconductivity [10,17–19]. For example, Nath et al. [20] described about photocatalytic decolorization of methylene blue by Se nanoparticle (NPs)-UV irradiation process. In the study conducted by Yang et al. [21], the chemically synthesized Se NPs have been successfully applied for removal of Congo red under UV irradiation. The single-crystalline Se nanorods (NRs), produced via a facile chemical reduction method, have been reported to exhibit excellent photocatalytic activities toward methylene blue after subjection to a short period of irradiation [15].

In the present study, the potential application of a photocatalytic system containing Se NPs biologically produced by a terrestrial actinomycete in combination with UV irradiation for decolorization of triphenylmethane dye, bromothymol blue (BTB) was evaluated. In addition, the effect of different parameters such as nanocatalyst concentration, H_2O_2 concentration, UV light intensity, and temperature on decolorization process was investigated.

2. Materials and methods

2.1. Chemicals

Selenium dioxide (SeO_2), nutrient broth, tryptone, hydrogen peroxide (H_2O_2) solution (30 wt.%), BTB, and *n*-Octanol were purchased from Merck chemicals (Darmstadt, Germany). All other chemicals and solvents used were of analytical grade.

2.2. Screening and identification of Se NPs-producer actinomycete

Isolation of actinomycete strains capable to produce Se NPs was performed according to the method described by Forootanfar et al. [22]. Briefly, 10 agricultural soil samples were collected from different locations in Kerman (57° 3′ 36′′ N, 30° 17′ 24′′ E), Iran and dried at room temperature. Thereafter, 20 mL of the sterile solution of sodium chloride (0.9%) containing Tween 80 (0.05%, v/v) was added to each soil sample (1 g), followed by shaking of the prepared suspension and filtering through Whatman No. 1 filter paper. The obtained soil extracts were then diluted and 100 μL of each filtrate was spread on a casein glycerol agar (CGA) plates [containing (g/L) casein, 0.3; glycerol, 10; NaCl, 2; KNO_3, 2; K_2HPO_4, 2; $MgSO_4 \cdot 7H_2O$, 0.05; $CaCO_3$, 0.02; $FeSO_4 \cdot 7H_2O$, 0.01 and agar 18] supplemented with SeO_2 (1.26 mM). In the next step, the prepared plates were incubated at 30°C until the actinomycete red colonies (an indicator of Se NPs production due to reduction of Se^{4+} ion into Se^0) appeared [23,24]. Subculturing of the obtained isolate was then performed in order to achieve axenic culture. Furthermore, positive colonies were cultured on CGA plates without SeO_2 to make sure about the absence of red pigment production (false positive) in the selected isolated bacterial strains.

Morphological and biochemical characteristics of the selected isolate were determined based on the Bergey's Manual of Determinative Bacteriology [25]. In addition, molecular identification of the selected isolate was performed after amplification of 16S rDNA gene using the forward primer of 27F (5′-AGAGTTT-GATCCTGGCTCAG-3′, positions 7–26 of the *E. coli*

16S rRNA gene), and the reverse primer of rp2 (5′-ACGGCTACCTTGTTACGACTT-3′, positions 1,513–1,494) followed by comparison of the obtained sequence by the BLAST software [26].

2.3. Production, purification, and characterization of biogenic Se NPs

The desired bacterial strain was cultivated in CG broth medium supplemented by Se^{4+} ions (100 μg/mL) for 5 d followed by harvesting the produced biomass by centrifugation (10,000 rpm for 5 min) and grinding the obtained cell pack in liquid nitrogen using a mortar and pestle. Afterward, the obtained blend was ultrasonicated at 100 W for 5 min and washed three times by ordinal centrifugation (10,000 rpm, 5 min) with 1.5 M Tris/HCl buffer (pH 8.3) containing 1% sodium dodecyl sulfate (SDS) and deionized water, respectively. The obtained pellets were then resuspended in deionized water, and the resulting suspension containing Se NPs and cell debris was collected. In the next step, *n*-Octanol (2.0 mL) was added to 4 mL of the obtained suspensions and the mixtures were shaken vigorously followed by separation of the resultant mixed phases using centrifugation at 5,000 rpm for 5 min and storing at 4°C for 24 h till the generated Se NPs observed at the bottom of the tubes. Thereafter, the lower and upper phases were discarded, and the precipitated NPs were washed with chloroform, ethyl alcohol, and distilled water, respectively. The purified Se NPs were then resuspended in deionized water and stored at 4°C before being used for characterization [27].

The transmission electron micrographs (TEM) of the biologically synthesized Se NPs were acquired by Zeiss Supra 55 VP TEM apparatus (operated at an accelerating voltage of 100 kV) equipped with an energy dispersive X-ray (EDX) microanalyzer after mounting of the purified Se NPs on carbon-coated copper TEM grids. The surface morphology of the prepared nanostructures was examined by scanning electron microscope (SEM, VEGAII TESCAN, acceleration voltage of 15 kV). In order to estimate the particle size distribution pattern of the biogenic Se NPs, an MS2000 Zetasizer (Malvern Instruments, Malvern, UK) was used. A Shimadzu UV–vis Double Beam PC Scanning spectrophotometer (UV-1800, Shimadzu CO, USA) was applied for recording the UV–visible spectrum of the purified Se NPs. The Fourier transform infrared spectroscopy (FTIR) spectrum of dried powder of Se NPs (in KBr pellet) was recorded by a Perkin Elmer instrument at a resolution of 4 cm^{-1}.

The X-ray diffraction (XRD) pattern of the Se NPs was obtained by a PW1710 diffractometer instrument (Philips, NY, USA) employing Cu-Kα radiation at a voltage of 40 kV and scanning range of Bragg angles from 20° to 80°. The Brunauer–Emmett–Teller (BET) method was also applied for measuring the surface area of the obtained Se NPs using the adsorption curve and BJH model, respectively.

2.4. Evaluation of photocatalytic activity of biogenic Se NPs

The potential photocatalytic activity of the biosynthesized Se NPs for removal of BTB was investigated by direct illumination of UV irradiation [in a UV cabinet equipped with three 15 W UV lamps with wavelength of 254 nm (Philips, Holland) which was placed 25 cm on the top and behind the batch photoreactor (Fig. 1)] into the reaction mixture containing BTB (180 μg/mL) dissolved in 50 mM citrate buffer (pH, 5), and Se NPs (64 μg/mL), for 60 min under continuous stirring followed by centrifugation of the taken samples (each 15 min to 60 min) at 5,000 g for 5 min and consequent determination of dye concentration using spectrophotometer at 431 nm. The decolorization percent was then calculated using the equation: Decolorization (%) = $[C_i - C_t/C_i] \times 100$; where C_i and C_t is the initial and final concentration of dye during photoirradiation process. In parallel, the photocatalytic activity of Se^{4+} ions was also evaluated by replacing the Se
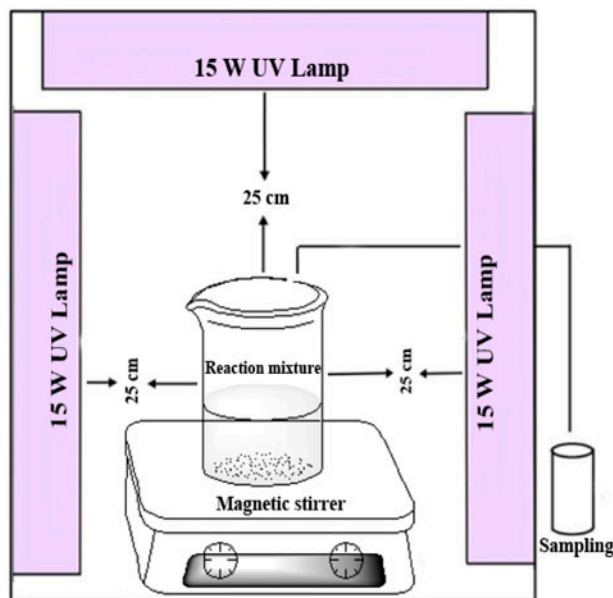

Fig. 1. The schematic view of UV cabinet applied for photocatalytic degradation. Three UV lamps placed above and behind the reaction mixture continuously stirred and sampling performed at desired times.
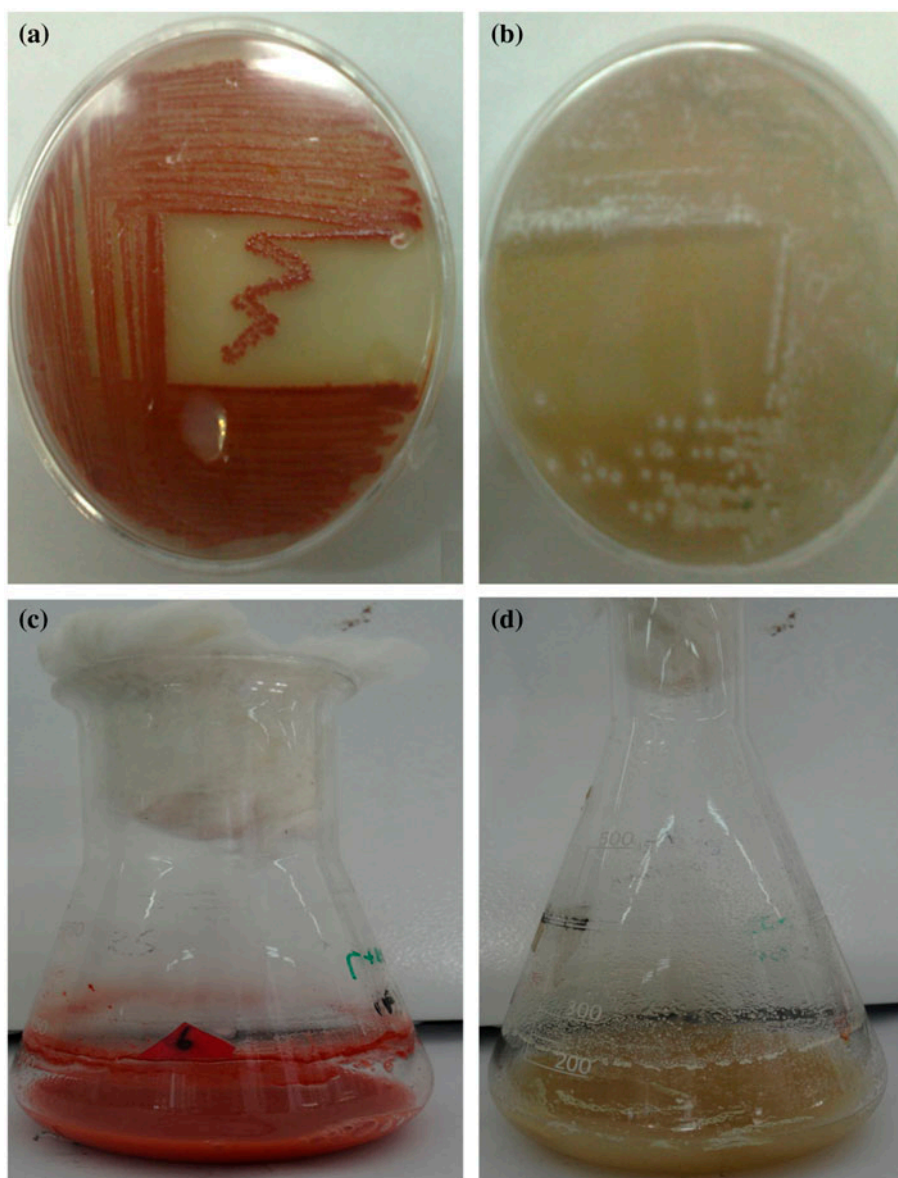
Fig. 2. Cultivation of *S. griseobrunneus* strain FSHH12 on CG agar plates: (a) with and (b) without Se^{4+} ions. Culture flasks of the selected isolate in the (c) presence and (d) absence of SeO_2 after incubation at 30℃.

NPs with the same concentration of SeO_2 solution in above-mentioned reaction mixture. In addition, the effect of variable parameters including Se NPs or SeO_2 concentrations (64–4 µg/mL), light intensity (15, 20, 25, and 30 W/m^2), temperature (25, 30, 35, 40, 45, and 50℃), and hydrogen peroxide concentration (0.1–0.4 M) on decolorization process was also evaluated.

2.5. Statistical analysis

After performing of all above-mentioned experiments in three independent replicate, the mean ± standard deviation of the obtained results were reported. Thereafter, independent sample *t*-test and one-way analysis of variance (ANOVA) with Dunnett's T3 *post hoc* test (SPSS 15.0, SPSS Inc) were used to calculate statistical significance between mean values (probability values < 0.05).

3. Results and discussion

3.1. Isolation and identification of Se NPs-producing bacterial strain

Out of 30 actinomycte bacterial strains isolated from collected soil samples, the ability of 3 isolates for
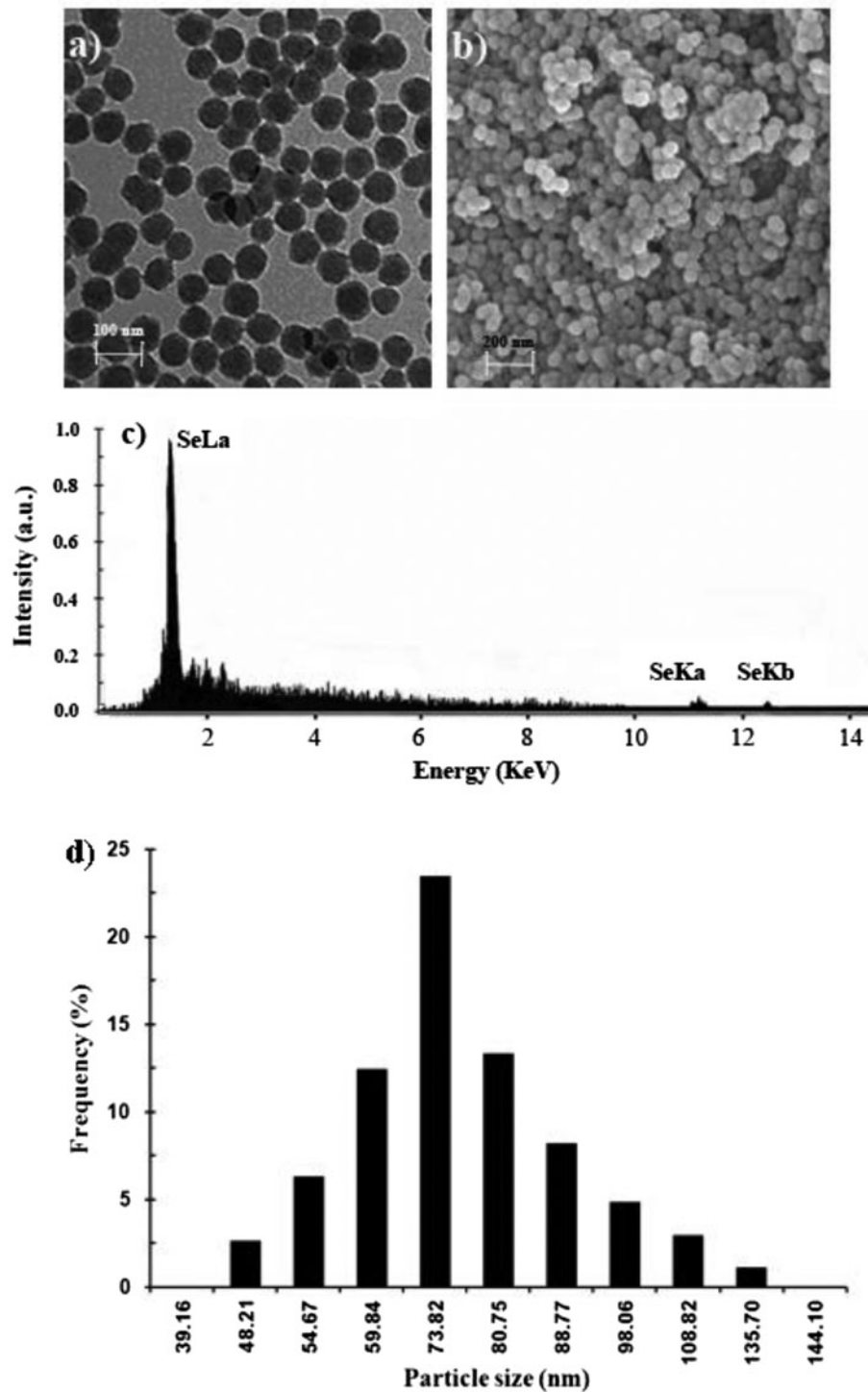
Fig. 3. (a) TEM, (b) SEM, (c) EDX, and (d) particle size distribution pattern of the purified Se NPs produced by the terrestrial actinomycete *S. griseobrunneus* strain FSHH12.

reduction of Se ions was confirmed by developing red colony on the CG agar plate containing Se^{4+} among which the isolate H12 was found to form such reduction more rapidly (Fig. 2(a)) compared to other two

isolates. Cultivation of the selected isolate on CG agar plate in the absence of SeO_2 (Fig. 2(b)) showed that microbial-assisted reduction of Se^{4+} and not the production of pigment was responsible for development
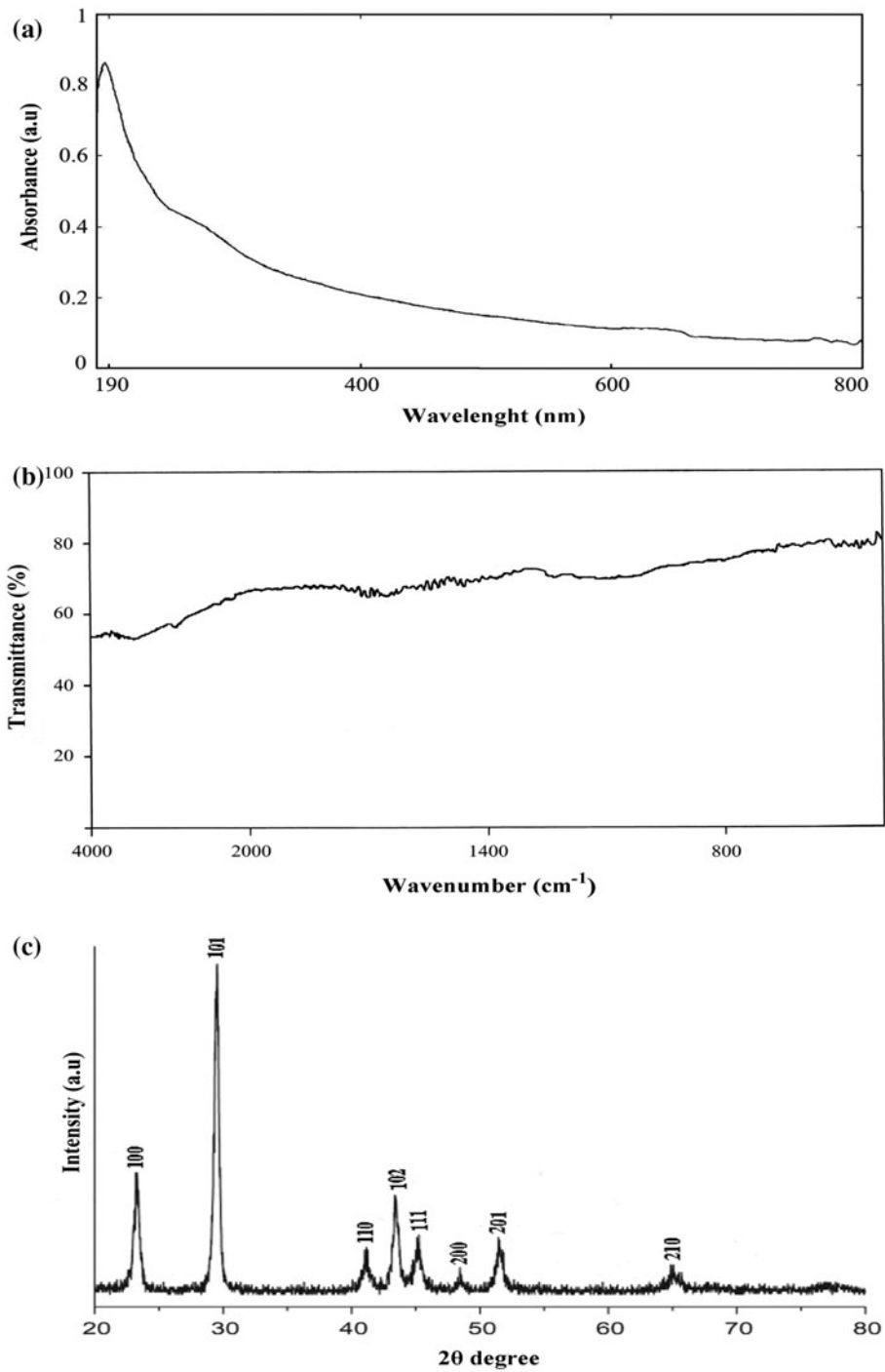
Fig. 4. (a) UV–visible spectroscopy, (b) FTIR, and (c) XRD pattern of the biogenic Se NPs.

of red colony. Same results were obtained when the selected isolate was cultured in CG broth medium in the presence (Fig. 2(c)) and absence (Fig. 2(d)) of Se^{4+} ions. Khiralla and El-Deeb [28] observed similar orange–red color development when SeO_2 solution (1 mM) was treated with the culture broth of *Bacillus*

licheniformis for 48 h. They ascribed such color change to the excitation of surface plasmon vibrations of the Se NPs and launched it as a convenient spectroscopic signature of Se NPs formation.

Morphological evaluation of the isolate H12 introduced it as a Gram-positive and filamentous bacterial
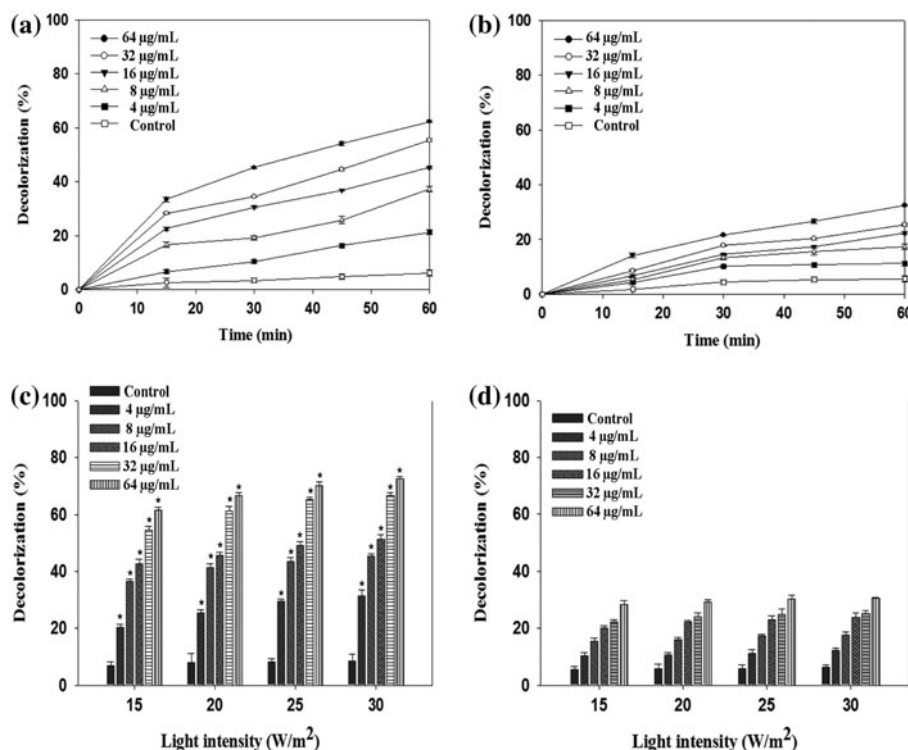
Fig. 5. Decolorization profile of BTB assisted by (a) biologically synthesized Se NPs and (b) SeO_2 under UV illumination (15 W) during 60 min incubation. The effect of light intensity on photocatalytic decolorization of (c) biogenic Se NPs and (d) SeO_2 at different concentration. Obtained means were analyzed by ANOVA with Dunnett's T3 *post hoc* test (*, *p*-value < 0.05).

strain formed floccose and powdery or a velvety colony on CG agar plate. The obtained results of the biochemical tests of the selected isolate are summarized in Table 1. After alignment of the amplified 16S rDNA gene of the isolate H12 using the BLAST software (GenBank, NCBI), 99% identity to *Streptomyces griseobrunneus* was acquired and the 1,433 bp targeted gene was recorded in GenBank under accession number of KC626002.

The unique physicochemical characteristics of Se such as thermo-conductivity, anisotropy, and high photoconductivity especially at nanoscale have gained the global attention to introduce more efficient methods for synthesis of Se NPs either via physicochemical or biological procedures [29]. Biosynthesis of Se NPs using either bacterial or fungal strains has been launched as an eco-friendly method supplying nanostructures with excellent characteristics [30,31]. For example, Ramya et al. [24] isolated a bacterial strain (designated as *Streptomyces minutiscleroticus* M10A62) from a magnesite mine able to produce Se NPs in the range of 10–250 nm. In the study conducted by Zhang et al. [32], the bacterial strain *Pseudomonas alcaliphila* able to synthesize spherical selenium nanostructure particles with diameters in the range of 50–500 nm was isolated from soil samples. Zare et al. [30] applied the culture broth of *Aspergillus terreus* toward SeO_2 for biosynthesis of Se NPs with the average size of 47 nm.

3.2. Purification and characterization of biogenic Se NPs

In the present study the biogenic Se NPs was successfully purified by the two-phase partitioning system using *n*-octyl alcohol/water. This was clearly observed from the TEM, SEM images, and EDX micro analysis of the well-dispersed and spherical-shaped purified nanostructures illustrated in Fig. 3(a)–(c). The particle size distribution pattern of the purified Se NPs (Fig. 3(d)) showed that they were in the range of 48.2–135.7 nm, and NPs in the size of 73.8 nm were the most frequent particles. The same result was reported by Forootanfar et al. [22] who applied similar procedure for purification of biogenic Se NPs produced by the terrestrial actinomycete *S. microflavus*. They obtained spherical-shaped nanoparticles with the size range of 28–123 nm [22]. The extracellular biogenic Se NPs produced by *S. minutiscleroticus* M10A62
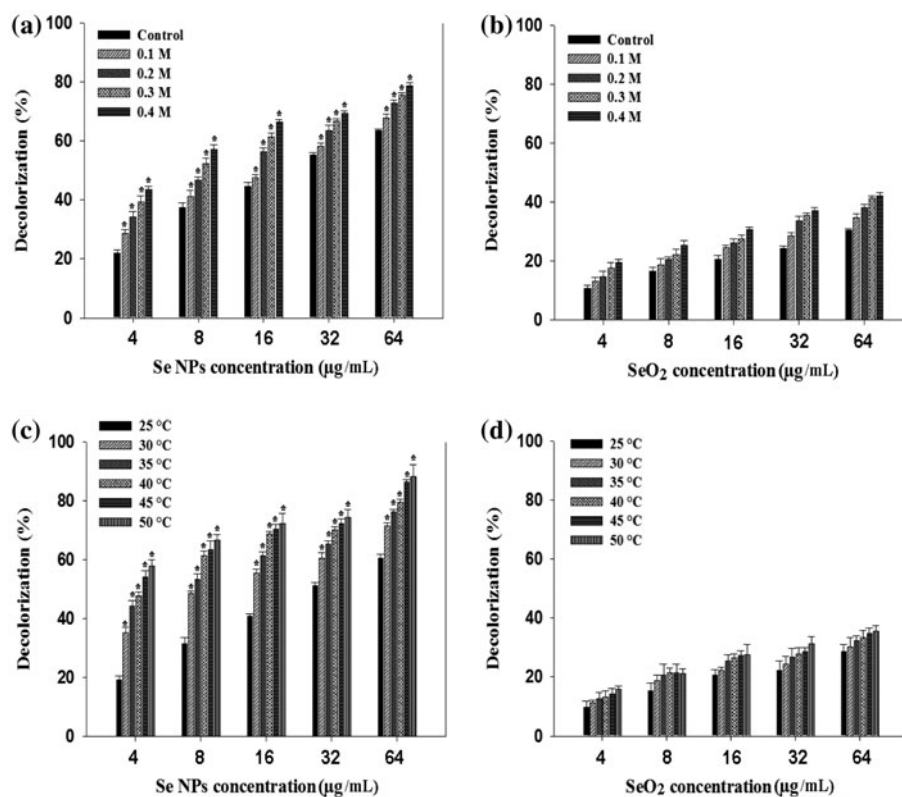
Fig. 6. Influence of H_2O_2 concentration (0–0.4 M) on photocatalytic decolorization of BTB assisted by (a) biogenic Se NPs and (b) SeO_2. Effect of reaction temperature (25–50°C) on photocatalytic decolorization of BTB assisted by (c) biogenic Se NPs and (d) SeO_2. Significant values (*, *p*-value < 0.05) were attained after ANOVA analysis with Dunnett's T3 *post hoc* test.

was found to be spherical nanostructures with the size range of 100–250 nm [24]. Wang et al. [23] employed a one-step procedure for preparation of spherical shaped Se NPs (average particle size of 25 nm) decorated by the water-soluble derivative of *Ganoderma lucidum* polysaccharides.

The obtained results of UV–visible spectroscopic analysis of the biogenic Se NPs in the present study (Fig. 4(a)) were in accordance with those reported by Forootanfar et al. [22] who applied *S. microflavus* for synthesis of Se nanostructures. Conversely, Ramya et al. [24] observed a maximum absorbance of 510 nm in the UV–visible spectrum of the biologically synthesized Se NPs produced by *S. minutiscleroticus* M10A62. This evidenced that Se produced by various selenium utilizing microorganisms represented different physicochemical characteristics.

The FTIR spectrum of the produced nanostructures in the present study (Fig. 4(b)) didn't exhibit any typical and strong absorption band corresponding to the functional groups on the surface of the biogenic Se NPs. Generally, mounting of proteins and biological

compounds on the surface of biologically derived nanostructures led to appearance of strong peaks in their FTIR spectrum [26]. For example, Khiralla and El-Deeb [28] observed strong broad peaks at 3,435, 2,750, 1,482, 1,325, 1,050, and 780 cm^{-1} assigned to OH or NH, –C–H, and aromatic groups of proteins and enzymes (might have formed a capping agents over the Se NPs) responsible for reduction of metal ions and their stabilization. FTIR analysis of the produced Se NPs in the study of Zhang et al. [33] revealed the appearance of stretching vibrations of –OH, –NH, –CH, and C–C bonds attributed to presence of chitosan assisted in the synthesis of nanostructures.

The related XRD pattern of the purified biogenic Se NPs in the present study (Fig. 4(c)) confirmed the formation of trigonal Se corresponded to the reported value of joint committee on powder diffraction standards (JCPDS File No. 06-0362). Our results were in agreement with the XRD spectrum of the Se NPs produced by the actinobacterium, *S. minutiscleroticus* M10A62 [24]. They ascribed the sharpening of the mentioned peaks to the spherical shape of the

Table 1
Biochemical characteristics of isolate H12

Characteristics	Results
Catalase production	+
Oxidase activity	−
Voges-Proskauer test	−
Methyl red test	−
Acid from	
D-Glucose	+
Maltose	+
Sucrose	+
Fructose	+
Hydrolysis of	
Casein	+
Gelatin	−
Starch	+
Utilization of citrate	+
Nitrate reduced to nitrite	−
Formation of	
Indole	+
Dihydroxyacetone	+
H_2S	+
Growth in NaCl (%)	
2.5	+
5	+
7.5	+
10	−
Growth at (°C)	
5	+
30	++
40	++
50	−

synthesized nanoparticles [24]. However, in the study conducted by Shakibaie et al. [27] the produced Se NPs by *Bacillus* sp. Msh-1 found to be amorphous and the related XRD pattern didn't exhibit any clear lattice parameters. The XRD analysis of the produced Se NPs using the free-cell supernatant of *B. licheniformis* showed three intense peaks at 2θ values of 23.78 (1 0 0), 29.8 (1 0 1), and 43.9 (1 0 2) indicating the face-centered cubic structure of red elemental selenium [28].

3.3. Photocatalytic decolorization process

As presented in Fig. 5(a) and (b), both the biologically synthesized Se NPs and bulk selenium dioxide assisted in the removal of BTB during 60 min UV illumination (15 W/m^2) in a time-dependent manner. In the case of the purified Se NPs, dye elimination was

maximally occurred (62.3%) at the concentration of 64 μg/mL after 60 min incubation (Fig. 5(a)) while SeO_2 (64 μg/mL) assisted to remove 32.5% of the applied dye at the same time (Fig. 5(b)). The dye removal percentage in the absence of SeO_2 or biogenic Se NPs was found to be 5.6 and 6.2%, respectively, after 60 min illumination of UV irradiation (15 W/m^2) (Fig. 5).

Compared to the conventional physical separation methods such as activation carbon adsorption, ultrafiltration, reverse osmosis, and gas sparging, etc. which transfers the pollutants to another phase and chemical techniques which almost suffer from time- and cost-consuming properties (due to requirement for high dosage of chemicals and production of large quantity of sludge), the AOP has received great interest due to its ability for mineralization of wide group of pollutants to CO_2 and H_2O through economical and environmentally friendly procedure [11,19]. Among different categories of AOPs (based on the methods applied for generation of hydroxyl radicals), the UV-based photocatalytic approach has been launched as an attractive choice because of its ability for degradation of desired xenobiotic without applying hazardous oxidant like ozone and chlorination [11,13]. Literature review revealed the critical role of semiconductors especially titanium dioxide (TiO_2) as photocatalyst in such valuable process [34,35]. The noticeable photoconductivity of elemental selenium (8×10^4 S/cm), especially at nanoscale launched it as an excellent catalyst in chemical synthesis and photocatalytic degradation of environmentally hazardous pollutants [15,21,36]. For instance, Dutta et al. [37] synthesized selenium-doped ZnO nanoparticles using a mechanochemical method and studied their photocatalytic activity toward trypan blue dye. They acquired higher dye degradation in the presence of selenium-doped ZnO compared to that of pristine ZnO which attributed to the higher reactive oxygen species (ROS) formation after dye treatment with selenium-doped ZnO [37]. Same results were reported by Lin et al. [38] where Te- and Se/Te-doped anatase TiO_2 nanorods were prepared and higher photocatalytic activity (generation of 2.5 and 4.5 times higher hydroxyl radicals compared to the commercial TiO_2) was determined for the as-synthesized nanostructures. In the present study, the potential application of SeO_2 and biologically synthesized Se NPs for elimination of BTB as a dye model was investigated. The obtained results revealed that biogenic Se NPs efficiently assisted to remove BTB (Fig. 5(a)) and increasing the concentration of applied photocatalyst positively affected the decolorization efficiency. In addition, decolorization pattern of bulk SeO_2 (Fig. 5(b)) represented lower

decolorization ability for Se^{4+} ions. In general, both the specific surface area of the applied photocatalyst and its concentration positively influenced the decolorization percent [11,19]. The obtained results of BET analysis in the present study revealed surface area of 42.2 m^2/g for biogenic Se NPs. Chiou and Hsu [15] synthesized single-crystalline Se nanorods (Se NRs) represented surface area of 46.6, 27.9, and 14.3 m^2/g with a facile chemical reduction approach (using $NaBH_4$ and carboxymethyl cellulose) and investigated their photocatalytic properties through methylene blue as a dye model. They found lower decolorization percent by decreasing the surface area of the prepared nanostructures and attributed it to decrease in the number of active sites accessible for photocatalysis [15]. In the study of Yang et al. [21] who applied chemically synthesized Se NPs for decolorization of congo red, it was found that the rate of dye decolorization decreased when the size of the Se NPs increased. They also reported that dye decolorization varies linearly with the nanoparticle concentration [21]. Same results were reported by Rajamanickam et al. [35] where the potential photocatalytic application of SeO_2/TiO_2 composite for degradation of the azo dye Sunset Yellow was studied. They observed an increase from 42.3 to 78.5% dye removal when the amount of the prepared photocatalyst increased from 50 to 250 mg.

3.4. Influence of UV intensity

The obtained results of BTB decolorization under four different UV intensities (15, 20, 25, and 30 W/m^2) for various concentrations of biologically synthesized Se NPs and Se^{4+} ions are illustrated in Fig. 5(c) and (d), respectively. In the case of Se NPs, significant increase of decolorization achieved by increasing the UV intensity (Fig. 5(c)) (*p*-value < 0.05). However, alteration of UV intensity in the presence of SeO_2 didn't have any significant effect on the decolorization percent of the applied dye (Fig. 5(d)).

The critical role of the UV light in the photocatalytic degradation of synthetic dyes and organic pollutants has been previously established [16]. For example, Nenavathu et al. [39] determined only 10% of trypan blue removal using Se-doped ZnO NPs in the absence of UV light which enhanced to 92.4% when UV irradiation (30 W) illuminated for 6 h. In fact, formation of electron–hole in photochemical reaction is strongly affected by light intensity. Increasing of the UV power (to a critical amount) enhances the photon absorption on the surface of catalyst and this increases the hydroxyl radical concentration and as a result the removal rate will increase [13].

3.5. Influence of H_2O_2

As presented in Fig. 6(a), addition of hydrogen peroxide to the reaction mixture containing biologically synthesized Se NPs significantly enhanced decolorization percent of BTB at all applied concentration with maximum removal percent of 78.6% achieved at concentration of 64 µg/mL of Se NPs and H_2O_2 concentration of 0.4 M (Fig. 6(a)) (*p*-value < 0.05). On the other hand, alteration of H_2O_2 concentration in the case of SeO_2 didn't significantly increase the removal efficiency (Fig. 6(b)).

It has been generally demonstrated that the presence of hydrogen peroxide enhance decolorization ability of photocatalytic cell [11]. Karimi et al. [40] who investigated on the photocatalytic degradation of two azo dyes using strontium titanate ascribed the positive influence of the H_2O_2 to the production of hydroxide radicals and prevention of recombination of electrons and holes. However, high dosage of H_2O_2 could negatively affect the photocatalytic-assisted decolorization procedure because of its hydroxyl radical scavenging effect [11,13].

3.6. Influence of temperature

As illustrated in Fig. 6(c), increasing of the reaction temperature from 25 to 50℃ enhanced decolorization of BTB from 60.4 to 88.3% in the presence of biogenic Se NPs (64 µg/mL) (*p*-value < 0.05). Significant change of decolorization percentage was also achieved in the presence of other concentration of Se NPs (Fig. 6(c)) (*p*-value < 0.05). However, change in decolorization pattern by increasing the Se^{4+} concentration was found to be insignificant (Fig. 6(d)).

Generally, elevation of the reaction temperature in photocatalytic process increases decolorization efficiency due to promotion of free radical production. The best temperature range for photodegradation was found to be 20–80℃ [11]. Higher (≤80℃) and lower (≥0℃) temperature negatively affected decolorization procedure due to the exothermic adsorption of pollutant on the catalyst surface and desorption of the product from the catalyst surface, respectively [11]. In the study performed by Karimi et al. [40], it was found that the highest photocatalytic activity of $SrTiO_3$ nanocomposite against two synthetic dyes of Direct Green 6 (a triazo dye) and Reactive Orange 72 (a monoazo dye) occurred when the reaction mixture incubated at 50℃. They attributed such positive effect of the temperature to the activation of the electron–hole at the interface and formation of more free radicals.

4. Conclusion

To sum up, the biologically synthesized Se NPs produced by the actinomycete *S. griseobrunneus* strain FSHH12 applied for decolorization of BTB under UV irradiation. The obtained results confirmed the potential application of the biogenic Se NPs compared to that of SeO_2 for removal of the triphenylmethane dye BTB. Nevertheless, further studies need be conducted to investigate action mechanisms of the produced Se NPs for dye elimination and identification of the probable metabolite(s).

References

[1] H. Forootanfar, A. Moezzi, M. Aghaie-Khouzani, Y. Mahmoudjanlou, A. Ameri, F. Niknejad, M.A. Faramarzi, Synthetic dye decolorization by three sources of fungal laccase, J. Environ. Health Sci. Eng. 9 (2012) 10 pages.
[2] S.D. Ashrafi, S. Rezaei, H. Forootanfar, A.H. Mahvi, M.A. Faramarzi, The enzymatic decolorization and detoxification of synthetic dyes by the laccase from a soil-isolated ascomycete, *Paraconiothyrium variabile*, Int. Biodeterior. Biodegrad. 85 (2013) 173–181.
[3] S. Rezaie, H. Tahmasbi, M. Mogharabi, A. Ameri, H. Forootanfar, M.R. Khoshayand, M.A. Faramarzi, Laccase-catalyzed decolorization and detoxification of Acid Blue 92: Statistical optimization, microtoxicity, kinetics, and energetic, J. Environ. Health Sci. Eng. 13 (2015) 9.
[4] L. Liu, J. Zhang, Y. Tan, Y. Jiang, M. Hu, S. Li, Q. Zhai, Rapid decolorization of anthraquinone and triphenylmethane dye using chloroperoxidase: Catalytic mechanism, analysis of products and degradation route, Chem. Eng. J. 244 (2014) 9–18.
[5] M.H. Dehghani, P. Mahdavi, Removal of acid 4092 dye from aqueous solution by zinc oxide nanoparticles and ultraviolet irradiation, Desalin. Water Treat. 54 (2015) 3464–3469.
[6] S.S. Mirzadeh, S.M. Khezri, S. Rezaei, H. Forootanfar, A.H. Mahvi, M.A. Faramarzi, Decolorization of two synthetic dyes using the purified laccase of *Paraconiothyrium variabile* immobilized on porous silica beads, J. Environ. Health Sci. Eng. 12 (2014) 9 pages.
[7] R.G. Saratale, G.D. Saratale, J.S. Chang, S.P. Govindwar, Bacterial decolorization and degradation of azo dyes: A review, J. Taiwan Inst. Chem. Eng. 42 (2011) 138–157.
[8] E. Brillas, C.A. Martínez-Huitle, Decontamination of wastewaters containing synthetic organic dyes by electrochemical methods. An updated review, Appl. Catal. B Environ. 166–167 (2015) 603–643.
[9] S.D. Marathe, V.S. Shrivastava, Removal of hazardous Ponceau S dye from industrial wastewater using nano-sized ZnO, Desalin. Water Treat. 54 (2015) 2036–2040.
[10] P. Li, Y. Song, S. Wang, Z. Tao, S. Yu, Y. Liu, Enhanced decolorization of methyl orange using zero-valent copper nanoparticles under assistance of hydrodynamic cavitation, Ultrason. Sonochem. 22 (2015) 132–138.
[11] H. Zangeneh, A.A.L. Zinatizadeh, M. Habibi, M. Akia, M. Hasnain Isa, Photocatalytic oxidation of organic dyes and pollutants in wastewater using different modified titanium dioxides: A comparative review, J. Ind. Eng. Chem. 26 (2015) 1–36.
[12] M.Q. Cai, X.Q. Wei, Z.J. Song, M.C. Jin, Decolorization of azo dye Orange G by aluminum powder enhanced by ultrasonic irradiation, Ultrason. Sonochem. 22 (2015) 167–173.
[13] U.G. Akpan, B.H. Hameed, Parameters affecting the photocatalytic degradation of dyes using TiO_2-based photocatalysts: A review, J. Hazard. Mater. 170 (2009) 520–529.
[14] A. Franco, M.C. Neves, M.M.L. Ribeiro Carrott, M.H. Mendonca, M.I. Pereira, O.C. Monteiro, Photocatalytic decolorization of methylene blue in the presence of TiO_2/ZnS nanocomposites, J. Hazard. Mater. 161 (2009) 545–550.
[15] Y.D. Chiou, Y.J. Hsu, Room-temperature synthesis of single-crystalline Se nanorods with remarkable photocatalytic properties, Appl. Catal. B: Environ. 105 (2011) 211–219.
[16] W.K. Jo, R. Tayade, Recent developments in photocatalytic dye degradation upon irradiation with energy-efficient light emitting diodes, Chin. J. Catal. 35 (2014) 1781–1792.
[17] N. Srivastava, M. Mukhopadhyay, Biosynthesis of SnO nanoparticles using bacterium *Erwinia herbicola* and their photocatalytic activity for degradation of dyes, Ind. Eng. Chem. Res. 53 (2014) 13971–13979.
[18] S.H. Park, S.J. Kim, S.G. Seo, S.C. Jung, Assessment of microwave/UV/O_3 in the photo-catalytic degradation of bromothymol blue in aqueous nano TiO_2 particles dispersions, Nanoscale Res. Lett. 5 (2010) 1627–1632.
[19] A.R. Khataee, M.B. Kasiri, Photocatalytic degradation of organic dyes in the presence of nanostructured titanium dioxide: Influence of the chemical structure of dyes, J. Mol. Catal. A: Chem. 328 (2010) 8–26.
[20] S. Nath, S.K. Ghosh, S. Panigahi, T. Thundat, T. Pal, Synthesis of selenium nanoparticle and its photocatalytic application for decolorization of methylene blue under UV irradiation, Langmuir 20 (2004) 7880–7883.
[21] L.B. Yang, Y.H. Shen, A.J. Xie, J.J. Liang, B.C. Zhang, Synthesis of Se nanoparticles by using TSA ion and its photocatalytic application for decolorization of cango red under UV irradiation, Mater. Res. Bull. 43 (2008) 572–582.
[22] H. Forootanfar, B. Zare, H. Fasihi-Bam, S. Amirpour-Rostami, A. Ameri, M. Shakibaie, M. Torabi Nami, Biosynthesis and characterization of selenium nanoparticles produced by terrestrial actinomycete *Streptomyces microflavus* strain FSHJ31, Res. Rev: J. Microbial. Biotechnol. 3 (2014) 47–53.

[23] J. Wang, Y. Zhang, Y. Yuan, T. Yue, Immunomodulatory of selenium nano-particles decorated by sulfated *Ganoderma lucidum* polysaccharides, Food Chem. Toxicol. 68 (2014) 183–189.

[24] S. Ramya, T. Shanmugasundaram, R. Balagurunathan, Biomedical potential of actinobacterially synthesized selenium nanoparticles with special reference to anti-biofilm, anti-oxidant, wound healing, cytotoxic and anti-viral activities, J. Trace Elem. Med. Biol. 32 (2015) 30–39.

[25] J.G. Holt, N.R. Krieg, P.H.A. Sneath, J.T. Staley, S.T. Williams, Bergey's Manual of Determinative Bacteriology, nineth ed., Williams and Wilkins, Baltimore, MD, 1994.

[26] J. Wood, K.P. Scott, G. Avgustin, C.J. Newbold, H.J. Flint, Estimation of the relative abundance of different bacteroides and prevotella ribotypes in gut samples by restriction enzyme profiling of PCR-amplified 16S rRNA gene sequences, Appl. Environ. Microbiol. 64 (1998) 3683–3689.

[27] M. Shakibaie, M.R. Khorramizadeh, M.A. Faramarzi, O. Sabzevari, A.R. Shahverdi, Biosynthesis and recovery of selenium nanoparticles and the effects on matrix metalloproteinase-2 expression, Biotechnol. Appl. Biochem. 56 (2010) 7–15.

[28] G.M. Khiralla, B.A. El-Deeb, Antimicrobial and anti-biofilm effects of selenium nanoparticles on some foodborne pathogens, LWT Food Sci. Technol. 63 (2015) 1001–1007.

[29] M.A. Faramarzi, A. Sadighi, Insights into biogenic and chemical production of inorganic nanomaterials and nanostructures, Adv. Colloid Interface Sci. 189–190 (2013) 1–20.

[30] B. Zare, S. Babaie, N. Setayesh, A.R. Shahverdi, Isolation and characterization of a fungus for extracellular synthesis of small selenium nanoparticles, Nanomed. J. 1 (2013) 13–19.

[31] H. Forootanfar, M. Adeli-Sardou, M. Nikkhoo, M. Mehrabani, B. Amir-Heidari, A.R. Shahverdi, M. Shakibaie, Antioxidant and cytotoxic effect of biologically synthesized selenium nanoparticles in comparison to selenium dioxide, J. Trace Elem. Med. Biol. 28 (2014) 75–79.

[32] W. Zhang, Z. Chen, H. Liu, L. Zhang, P. Gao, D. Li, Biosynthesis and structural characteristics of selenium nanoparticles by *Pseudomonas alcaliphila*, Colloids Surf., B: Biointerfaces 88 (2011) 196–201.

[33] C. Zhang, X. Zhai, G. Zhao, F. Ren, X. Leng, Synthesis, characterization, and controlled release of selenium nanoparticles stabilized by chitosan of different molecular weights, Carbohydr. Polym. 134 (2015) 158–166.

[34] H. Khan, D. Berk, Selenium modified oxalate chelated titania: Characterization, mechanistic and photocatalytic studies, Appl. Catal. A Gen. 505 (2015) 285–301.

[35] D. Rajamanickam, P. Dhatshanamurthi, M. Shanthi, Preparation and characterization of SeO_2/TiO_2 composite photocatalyst with excellent performance for sunset yellow azo dye degradation under natural sunlight illumination, Spectrochim. Acta, Part A: Mol. Biomol. Spectrosc. 138 (2015) 489–498.

[36] Y.Y. Gurkan, E. Kasapbasi, Z. Cinar, Enhanced solar photocatalytic activity of TiO_2 by selenium(IV) ion-doping: Characterization and DFT modeling of the surface, Chem. Eng. J. 214 (2013) 34–44.

[37] R.J. Dutta, B.P. Nenavathu, S. Talukdar, Anomalous antibacterial activity and dye degradation by selenium doped ZnO nanoparticles, Colloids Surf., B: Biointerfaces 114 (2014) 218–224.

[38] Z.H. Lin, P. Roy, Z.Y. Shih, C.M. Ou, H.T. Chang, Synthesis of anatase Se/Te-Tio$_2$ nanorods with dominant 100 facets: Photocatalytic and antibacterial activity induced by visible light, ChemPlusChem 78 (2013) 302–309.

[39] B.P. Nenavathu, A.V.R. Krishna Rao, A. Goyal, A. Kapoor, Synthesis, characterization and enhanced photocatalytic degradation efficiency of Se doped ZnO nanoparticles using trypan blue as a model dye, Appl. Catal. A: Gen. 459 (2013) 106–113.

[40] L. Karimi, S. Zohoori, M.E. Yazdanshenas, Photocatalytic degradation of azo dyes in aqueous solutions under UV irradiation using nano-strontium titanate as the nanophotocatalyst, J. Saudi Chem. Soc. 18 (2014) 581–588.